The Inelastic Scattering of 31-Mev Protons from Heavy Elements

R. M. EISBERG* AND G. IGO†
Radiation Laboratory, Department of Physics, University of California, Berkeley, California
(Received September 8, 1953)

Energy distributions, angular distributions, and total cross sections for the inelastic scattering of 31-Mev protons from four heavy elements, Pb, Au, Ta, and Sn, have been measured. Information was obtained at five scattering angles: 30°, 45°, 60°, 90°, and 135°. The energy distributions do not show the Maxwellian-like behavior which would be predicted on the basis of compound nucleus theory. The differential cross sections are strongly peaked forward, increasing by about a factor of ten as the scattering angle goes from 135° to 30°. The total cross sections all have values ranging from 0.25 barns for Sn, to 0.29 barns for Pb. A model has been proposed which is capable of giving a qualitative explanation of the results of the experiment. According to the model, the inelastic scattering occurs when the incident proton collides with the rim of a target nucleus.

I. INTRODUCTION

INELASTIC scattering of high-energy protons is a technique which has been used extensively in the past decade to investigate the energy structure of nuclei. The procedure involves bombarding thin targets of the element to be investigated with monoenergetic protons and, at some angle with respect to the incident beam, observing the energy distribution of the scattered protons.

When targets of low atomic number are used, the energy spectra of the scattered protons are usually found to consist of an elastically scattered group and several discrete groups of lower energy, corresponding to inelastic scattering.[1] In the center-of-mass system, the energy of the incident proton, less the energy of the inelastically scattered proton, must equal the energy absorbed by the target nucleus. Thus, from the observed laboratory energy spectrum of protons, one may infer information about the spectrum of energy levels of the target nucleus.

The density of energy levels of a nucleus, in the neighborhood of a particular excitation energy, increases as the excitation energy increases. Thus, at sufficiently high bombarding energies, it is found that the spectrum of the lower-energy inelastically-scattered protons is continuous (corresponding to excitation of the target nucleus to its continuum). Furthermore, as the atomic number of a nucleus increases, the average spacing of the energy levels of the nucleus decreases. Thus, using apparatus of moderate resolving power, one would expect that the observed energy spectrum of protons inelastically scattered from a heavy element would consist entirely of a continuous spectrum. The information that one would expect to obtain about the heavy elements from inelastic scattering, consequently, differs from that obtained about light elements. For the light elements, inelastic proton scattering provides the location of discrete energy levels—for the heavy elements, it could be expected to provide information about density of levels.

Most of the inelastic proton scattering experiments performed to date have used bombarding energies in the region of 4 to 8 Mev.[2–4] These experiments are limited to the investigation of the lighter nuclei in which the Coulomb barrier is lower than the bombarding energy. The Berkeley proton linear accelerator, which produces an intense, well-collimated beam of 31-Mev protons, is thus particularly well suited for inelastic scattering experiments with the heavy elements.

The results of several experiments involving the lighter nuclei, performed with 31-Mev protons, can be explained by the compound nucleus theory.[5,6] Consequently it would be reasonable to anticipate that the inelastic scattering of 31-Mev protons from heavy elements would also be a compound nucleus process. For such a compound nucleus process the energy distribution of inelastically scattered protons would be a Maxwellian (modified by the effect of the Coulomb barrier) corresponding to a temperature of the order of 1 Mev.[7,8] The angular distribution would be isotropic, and the total cross section would be very small because only protons in the high-energy tail of the Maxwellian distribution would be able to escape through the high Coulomb barrier of the heavy nucleus. On the other hand, any inelastic proton-scattering process in competition with the compound-nucleus process could easily dominate in this case since the compound-nucleus inelastic proton scattering cross section is so small.

The first experiments on the inelastic proton scattering from heavy elements were done several years ago at the Berkeley linear accelerator by Britten.[9] He observed the energy spectra of protons scattered at 90° from Pt and Pb. The observed energy spectra were

* Now at Brookhaven National Laboratory, Upton, New York.
† Now at Yale University, New Haven, Connecticut.
[1] E. H. Rhoderick, Proc. Roy. Soc. (London) **201**, 348 (1950). This paper contains an extensive bibliography of the earlier work on inelastic proton scattering from the light elements.
[2] Baker, Dodd, and Simmons, Phys. Rev. **85**, 1050 (1952).
[3] H. E. Gove and J. A. Harvey, Phys. Rev. **82**, 658 (1951).
[4] H. W. Fulbright and R. R. Bush, Phys. Rev. **74**, 1323 (1948).
[5] Levinthal, Martinelli, and Silverman, Phys. Rev. **78**, 199 (1950).
[6] S. N. Ghoshal, Phys. Rev. **80**, 939 (1950).
[7] V. Weisskopf, Phys. Rev. **52**, 295 (1937).
[8] L. Wolfenstein, Phys. Rev. **82**, 690 (1951).
[9] R. Britten, Phys. Rev. **88**, 283 (1952).

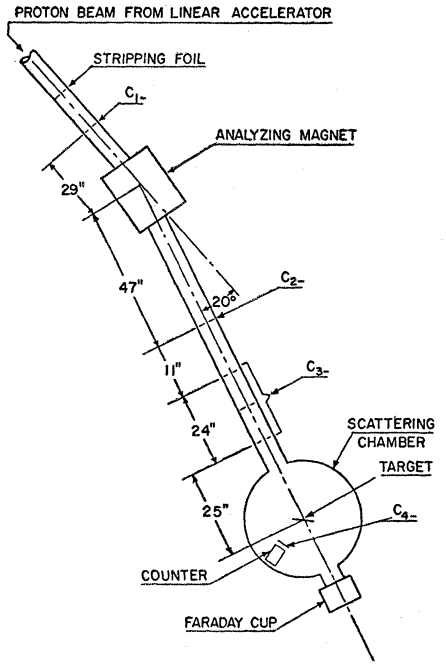

FIG. 1. Schematic diagram of the bombardment geometry.

not of the Maxwellian character predicted by compound nucleus theory, and the measured differential cross sections were at least an order of magnitude larger than the predictions of compound-nucleus theory.

The experiment reported in this paper is an amplification of an earlier experiment performed to confirm the results of Britten.[10] In the present experiment 30.6-Mev protons were scattered from four elements: Sn, Ta, Au, and Pb. Energy distributions of scattered protons were obtained, for each element, at each of six different angles: 15°, 30°, 45°, 60°, 90°, and 135°. The scattered protons were detected by a multiple-counter telescope consisting of three proportional counters and a sodium iodide scintillation counter. The detected particles traverse the three proportional counters, which obtain three samples of the particle's specific ionization and then stop in the scintillation counter, which measures their energy. By correlating the information obtained on the specific ionization with the measurement of the particle's energy, one is able to identify the mass of the detected particle.

II. EXPERIMENTAL TECHNIQUES

A. The Linear Accelerator

The Berkeley linear accelerator is ideally suited as a proton source for heavy-element inelastic scattering experiments. It produces a monoenergetic beam of 31-Mev protons confined to a very narrow bundle of small angular divergence. The beam is emitted in pulses of about 300 microseconds duration at a repetition rate of 15 cps. Thus, it has a very reasonable duty cycle (time "on" per second) of approximately $\frac{1}{2}$ percent. The available time-average beam, for the highly collimated geometry used, is of the order of 10^{-8} ampere, which is somewhat more than could be used in this experiment.

[10] R. M. Eisberg and G. J. Igo, Phys. Rev. **92**, 537 (1953).

B. Bombardment Geometry

Figure 1 shows the geometry of collimators, target, counter, and Faraday cup as used in the experiment. The stripping foil consists of a $\frac{1}{4}$-mil aluminum foil which is inserted in the beam ahead of the analyzing magnet. Its purpose is to break up singly-ionized hydrogen molecules, which can be produced at about 16 Mev by the linear accelerator, into two 8-Mev protons which are then removed from the beam by the analyzing magnet. The collimator C_1 is used to control the beam current. It is generally set at about $\frac{1}{8}$ in. by $\frac{1}{8}$ in. After passing through the analyzing magnet, the beam is collimated roughly by C_2, which is set at about $\frac{3}{16}$ in. by $\frac{3}{16}$ in. Collimator C_3 consists of three carbon disks spaced one foot apart. The first disk has a $\frac{1}{8}$-in. hole; the second and the third have $\frac{3}{16}$-in. holes. The collimator is constructed so that the three holes are very accurately coaxial. The first disk gives the beam its final shape. The second and the third disks do not scrape the main beam but act as baffles to remove protons which are scattered from the edges of the first disk. Carbon is used in C_3 because its low Z gives a favorable ratio of stopping power to multiple Coulomb scattering and because its high (p,n) threshold makes it a poor source of background neutrons.

The targets consist of thin foils, $\frac{3}{4}$ in. high and $1\frac{1}{4}$ in. wide, placed at the center of the scattering chamber at 45° to the incident beam. The counter telescope may be set at any desired angle with respect to the incident beam. Particles scattered from the target are required to pass through one more collimator, C_4, before entering the detecting counters. This collimator, which determines the solid angle involved in the calculation of cross sections from the data, is mounted at the front of the counter telescope. It consists of a $\frac{3}{32}$-in. hole in a steel plate at $5\frac{11}{16}$ in. from the center of the target. This defines the solid angle to be 2.13×10^{-4} steradian. To monitor the beam passing through the target, a Faraday cup is mounted on the exit port of the scattering chamber. The Faraday cup, the scattering chamber, and the pipe containing the collimators are all evacuated.

C. The Scattering Chamber

Figure 2 shows a schematic diagram of the scattering chamber. The evacuated volume consists of a circular cylinder 2 ft in diameter and 1 ft high. The incident beam passes through the chamber eight inches above the base. The counters are mounted on a circular table which is capable of rotating through 360° and is driven by a motor. Along the vertical axis of the cylinder is a shaft which supports a frame which can hold eight

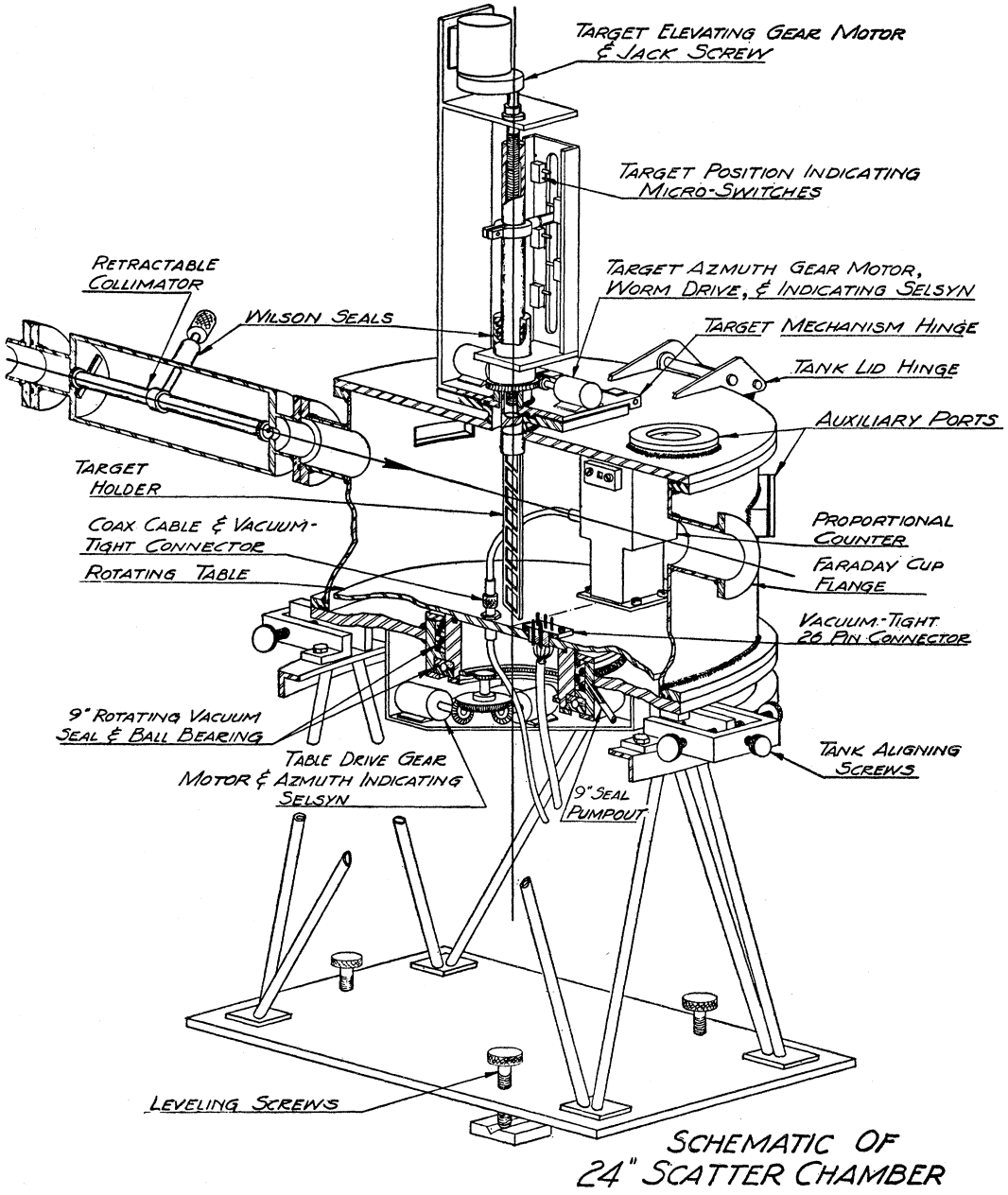

FIG. 2. Schematic diagram of the 24-in. scattering chamber.

targets. Motors drive the shaft up and down and cause it to rotate. The azimuthal and vertical location of the target holder and the azimuthal position of the table are indicated at the remote control panel by a system of selsyns and microswitches. The scattering chamber may be evacuated to a pressure of the order of 10^{-5} mm of Hg by means of a self-contained pump unit.

D. Beam Integration

The beam passing through the target was collected in a Faraday cup mounted on the exit port of the scattering chamber. So that secondary electrons might be prevented from escaping from the Faraday cup, two large Alnico horseshoe magnets were placed to provide a transverse field of several hundred gauss over the surface of the cup struck by the beam. A second pair of magnets placed in front of the Faraday cup served to prevent any electrons that might be in the beam from entering the cup.

The charge collected on the Faraday cup was measured by a feed-back integrating electrometer. The feed-back voltage V is applied to a recording

TABLE I. Areal density of targets.

Element	Areal density, mg/cm²
Sn	37.5
Ta	27.9
Au	36.9
Pb	39.2

voltmeter. The operation of the feed-back circuit is such that the effect of the capacitance of the Faraday cup and the cable is negligible compared with the capacitance C of the condenser in the electrometer circuit. Consequently the charge Q collected is given by the expression $Q=CV$. C was measured to be 0.101 microfarad.

E. Targets

Four targets were used in the experiment: Sn($Z=50$), Ta($Z=73$), Au($Z=79$), and Pb($Z=82$). For maximization of the ratio of scattered protons to background, the foils were made as thick as possible, subject to two restrictions. First, multiple Coulomb scattering of the incident beam by the target could not be so great that the available Faraday cup would not be large enough to intercept the beam. Second, the targets could not be so thick that the uncertainty introduced in determining the energy of the lowest energy protons expected, due to the uncertainty in their point of origin in the target, was the determining factor in the energy resolution of the experiment. It happened that either of these criteria, taken alone, gave about the same result for the optimum target thickness. The optimum areal density came out to be 40 mg/cm². The measured areal densities are given in Table I. (These figures include a factor of $\sqrt{2}$ arising from the fact that the targets were placed at an angle of 45° to the incident beam.)

F. The Scintillation Counter

Protons scattered from the targets first pass through the proportional counters and then enter the thallium-activated sodium iodide crystal, which is thick enough to stop the most energetic protons encountered. The scintillation crystal is observed by a RCA 5819 photomultiplier tube.

The greatest difficulty in using sodium iodide as a scintillator arises from the fact that it is deliquescent. For the purpose of overcoming this difficulty, the following technique was used. A stubby quartz light pipe in the shape of a truncated cone is cemented, in optical contact, to the face of the 5819 photomultiplier. In a dry box, the sodium iodide crystal is cleaved to the shape of a cube, approximately $\frac{5}{8}$ in. on an edge. The crystal is then cemented, in optical contact, to the flat face of the light pipe with a cement known as Bonding Agent R-313 (made by Carl H. Biggs Company, Los Angeles, California). This cement is ideal for the purpose. It dries in several hours after the addition of a hardener. When dry, it is hard and clear. It does not attack sodium iodide. Next a cap of $\frac{1}{4}$-mil aluminum foil is placed over the crystal and the slant sides of the light pipe. This serves to direct all the light to the photomultiplier. Then a vacuum tight housing is slipped over the assembly and sealed to the end of the 5819 by means of a gum-rubber gasket. The device is then removed from the dry box, and the housing is evacuated. Protons can pass through a thin window in the housing and enter the crystal. By use of this technique, the crystal will be preserved indefinitely.

G. The Proportional Counters

Before entering the scintillation counter, the scattered protons traverse a set of three proportional counters. Each counter consists of a grounded cylindrical shell, $\frac{3}{4}$ in. in internal diameter and 3 in. long, with a 0.003-in. stainless-steel wire located along the axis of the cylinder. The wire is supported at each end by disks of Teflon and is maintained at a positive potential of 1800 volts. The cylindrical volume is filled to one atmosphere with a mixture of 96 percent A and 4 per cent CO_2. The narrow bundle of scattered protons passes through the counter perpendicular to its axis and straddling the wire.

The mean rate of energy loss of a particle in traversing matter can be expressed as a function of its kinetic energy, charge, and mass. Thus, at kinetic energies of 31 Mev, a deuteron will have a mean rate of energy loss 1.7 times larger than that of a proton and about 25 times larger than that of an electron. As the kinetic energy is decreased, the ratio of the mean energy loss of deuterons compared to protons remains about 1.7. Consequently, by correlating the heights of pulses from the scintillation counter and one of the proportional counters, it should be possible to determine the mass of the particle detected. In practice it is not possible to do this with use of only one proportional counter because of the large statistical fluctuations in the energy loss of charged particles of energies encountered in this experiment in traversing a proportional counter of a reasonable thickness.[11] The frequency distribution of the energy loss of 31-Mev protons in traversing a $\frac{3}{4}$-in. counter is a skew, bell-like curve with a full width, at half-maximum, of about 50 percent and with a very pronounced tail extending to the high energy losses.[12] This distribution (in particular, the presence of the tail) is too broad to allow adequate resolution of protons and deuterons. However, by use of three proportional counters to sample the ionization of the particle three times, it is possible to achieve a much more accurate estimate of the mean ionization of the particle. This information is treated by sending the three proportional counter pulses into a circuit which selects the smallest pulse. The output of this circuit is then used to represent

[11] B. Rossi, *High Energy Particles* (Prentice-Hall, Inc., New York, 1952), p. 29.

[12] Igo, Clark, and Eisberg, Phys. Rev. 89, 879 (1953).

the mean ionization of the particle. This method is described in detail elsewhere in the literature.[13]

The three proportional counters are machined from a solid block of brass and are evacuated and filled from a common port. The entrace window is a $\frac{1}{4}$-mil Al foil, $\frac{1}{8}$ in. in diameter. There are no foils between the first and second or the second and third counters. The exit window of the third counter and the entrance window of the scintillation counter are sufficiently larger than $\frac{1}{8}$ in. so that multiple Coulomb scattering, of the lowest energy particles detected, in the entrance window and counter gas will not deflect them out of the counter telescope.

H. The Electronics

Figure 3 shows a block diagram of the electronic setup used in the experiment. The detected protons traverse proportional counters (PROP) 2, 3, and 4 in succession and then stop in the scintillation counter (XTAL). The pulses from the counters are first fed into shorted delay line clipping units (CLIP) which provide rectangular pulses, 1 microsecond long, whose heights are proportional to the size of the counter pulses. The pulses are then sent through preamplifiers (PA) and linear amplifiers (LA).

The scintillation counter pulses are fed into a one-channel pulse-height analyzer (PHA). This unit has two outputs: integral and differential. A pulse will appear in the integral output whenever the scintillation counter pulse is higher than a level determined by the lower discriminator. The differential output will deliver a pulse whenever the scintillation counter pulse is higher than the level determined by the lower discriminator and lower than the level determined by the higher discriminator. The integral and differential outputs are fed into units containing a discriminator and a circuit giving a rectangular output pulse of variable length (DISC and GATE).

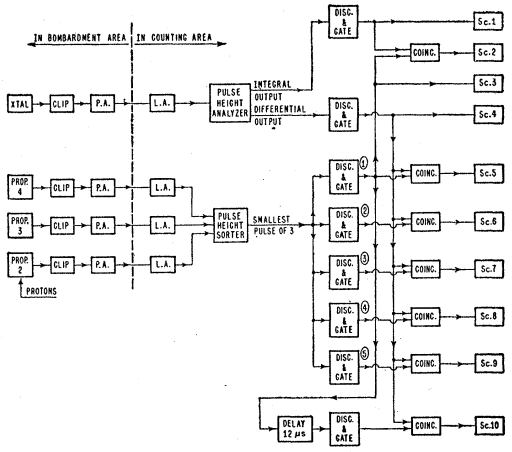

FIG. 3. Block diagram of the electronics.

[13] G. Igo and R. Eisberg, Rev. Sci. Instr. (to be published).

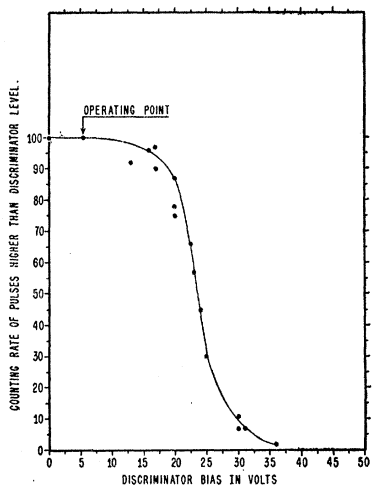

FIG. 4. Integral pulse-height distribution plateau of energy losses.

The three proportional counter pulses are fed into a pulse-height sorter which provides an output pulse whose height is proportional to the height of the smallest of the three input pulses. This device is essentially a Rossi coincidence circuit. The output of this circuit is fed to the inputs of five DISC and GATE units. Unit number 1 is set so that it will produce an output pulse whenever a particle of ionization equal to, or greater than, that of a 31-Mev proton traverses the proportional counters. The discriminators of unit 2 through 5 are set at successively higher levels and are used to run a five-point pulse-height analysis on the proportional counter pulses.

The outputs of DISC and GATE 1 through 5 are put into coincidence with pulses from the PHA differential output in the coincidence circuits (COINC). The output of DISC and GATE number 1 is also put into coincidence with the PHA integral output. In addition, the output of DISC and GATE number 1 is used to trigger a delay circuit which in turn produces a pulse of the same duration as the pulse from DISC and GATE 1 but which is delayed by 12 microseconds. This delayed pulse is put into coincidence with the PHA differential-output pulse and is used to determine the contribution of accidental coincidences to the counts recorded by the coincidence circuit fed by the PHA differential output and the output of DISC and GATE 1. Finally the unmixed differential and integral PHA counts are recorded as well as the counting rate of DISC and GATE 1.

The operation of this circuitry will be further explained in the following sections.

I. Proportional Counter Plateaus

The DISC and GATE number 1 is set so that it will produce an output pulse whenever a heavily ionizing particle traverses the three proportional counters. To do this, the counter telescope is set at some forward angle, where most of the particles entering the telescope are elastically scattered protons. The pulse-height

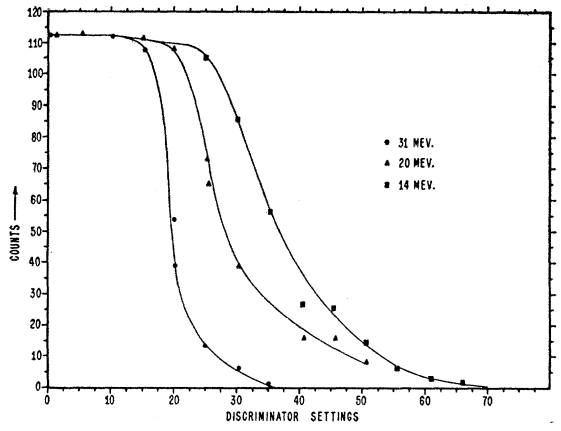

FIG. 5. Integral pulse-height distribution plateaus for three energies of detected particles.

analyzer is set so that it will produce a pulse in its differential output channel when an elastically scattered proton enters the counter telescope. The counting rate of the output pulses of the coincidence circuit fed by DISC and GATE 1 and the PHA differential output is measured as a function of the bias on the discriminator of DISC and GATE 1. When the beam intensity is kept at a reasonable level, a sharply rising plateau is obtained, such as is shown in Fig. 4. This curve, when differentiated, gives the frequency distribution of pulse heights due to 31-Mev protons from the circuit which selects the smallest of the three proportional counter pulses. The derivative is a Gaussian-like curve with a full width at half-maximum of about 30 percent, which is appreciably narrower than what would be obtained using only one counter. The bias of DISC and GATE 1 is set so that the coincidence rate is well up on the plateau, as indicated in Fig. 4. The unit will then produce a gate whenever a 31-Mev proton traverses the proportional counters. Since the specific ionization of a particle increases with decreasing energy and increasing mass, DISC and GATE 1 will also produce a gate whenever a lower-energy proton or deuteron traverses the proportional counters.

III. EXPERIMENTAL RESULTS

A. Search for Deuterons

At each setting of the pulse-height analyzer, corresponding to a particular energy of the detected particles, the biases of the five DISC and GATE units were set at progressively higher levels so as to obtain an integral pulse-height analysis on the ionization pulses. The presence of deuterons would then be distinguished by the presence of a double-step plateau.

Figure 5 shows ionization pulse plateaus for particles of 31 Mev, 20 Mev, and 14 Mev, from a lead target at 60°. The knees of the plateaus can be seen to fall at a pulse height which is inversely proportional to the energy of the particles. Since at 31 Mev all the particles must be protons, then the other plateaus must be due primarily to protons with no large contamination of deuterons. Five-point discriminator plateaus were run on each two-Mev energy channel for each element, at each angle. No deuterons were observed from any of the elements in large numbers. Any peaked distribution of deuterons would have been observed; and if the deuterons were distributed uniformly at all energies, they must not represent more than about 10 percent or 15 percent of all particles counted.

As a qualitative check on the identification of the particles, a photographic method was employed to determine the mass of the particles. The specific ionization is proportional to the ratio of the mass to the energy, so the product of the scintillation counter pulse height and the smallest pulse height of three proportional counter pulse heights is proportional to the mass of the particle. The pulses from the counters were displated on the verticle and horizontal plates of an oscilloscope. The oscilloscope beam was gated on by the proportional counter pulse. This gave a dot of light each time a particle traversed the counter telescope, whose abscissa is proportional to the ionization and whose ordinate is proportional to the energy of the particle. Particles of different masses should fall on separate hyperbolas. Figure 6 shows some of the film data. The elastically scattered protons fall in the prominent spot. No large number of particles lie off the proton hyperbola.

B. Energy Spectra

Figure 7 shows a typical energy spectrum—lead at 90°. The abscissa is particle energy, corrected for window absorption, and the ordinate is counting rate. The large peak at 31 Mev contains the elastically

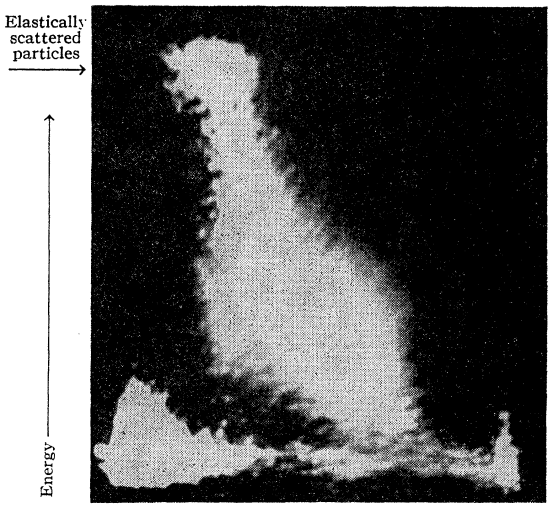

FIG. 6. Photograph of energy losses *vs* energies of particles emitted from a heavy element.

scattered protons. The hump, below the solid line, contains the inelastically scattered protons. Curve *a*, which fuses into the solid curve at about 18 Mev, represents the energy distribution of *all* pulses in the sodium iodide crystal. Curve *b*, which fuses into the solid curve at about 12 Mev, represents crystal pulses which are in time coincidence with a gate from DISC and GATE 1. Thus one sees that below about 15 Mev most of the crystal counts are due to background. The higher-energy background pulses are undoubtedly due to pile-up of the more numerous lower-energy pulses. Curve *c* represents the rate of accidental coincidences between crystal pulses, of a particular energy, and the gates from DISC and GATE 1. The accidentals are measured with the delayed coincidence setup shown in Fig. 3. The solid curve is the difference between curve *b* and curve *c*. It represents the coincident crystal pulses, with accidental coincidences subtracted out—thus the points on the solid curve give the counting rate of real scattered protons.

As the scattering angle decreases towards zero, the cross section for elastic scattering increases very rapidly. Consequently, the complete energy spectra will have a very different appearance at small angles. Figures 8 through 11 show energy spectra for Pb at all the other angles of observation. Figure 12 shows the inelastic spectra of Sn at five angles of observation.

C. Calculation of Cross Sections

Determining the differential cross sections from the energy spectra is simply a matter of counting the total

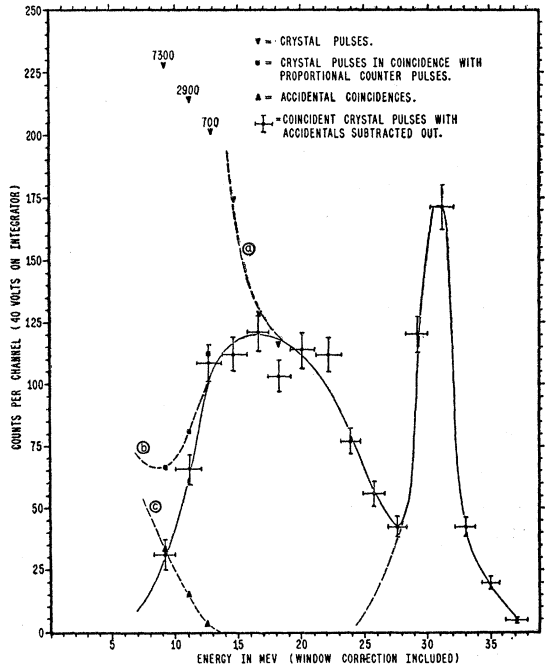

FIG. 7. Typical energy spectra of protons emitted at 90° from Pb bombarded by 31-Mev protons.

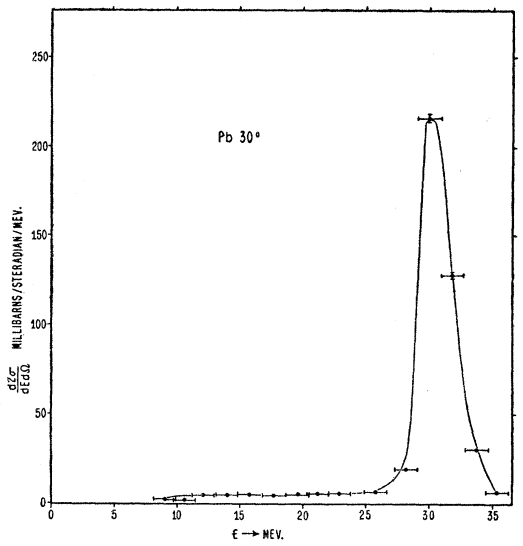

FIG. 8. Energy spectra of protons emitted by Pb at 30° when bombarded by 31-Mev protons.

number of inelastically scattered protons and multiplying by a factor determined by the number of nuclei per cm², the number of bombarding protons, and the solid angle accepted by the counter telescope. To determine the number of inelastically scattered protons it is necessary to take into account the finite resolving power of the scintillation counter for the elastically scattered protons (approximately 8 percent full width at half-maximum). The most reasonable method for doing this involves assuming the resolution curve for the instrument is symmetrical about its maximum point. The upper half of the elastic peak is reflected about its maximum, and the wing of the curve extending into the region of inelastically scattered protons is subtracted out. The reflection process is indicated in Fig. 7.

The differential cross section is defined by the equation

$$N_c = \frac{d\sigma}{d\Omega} \Delta\Omega N_n F,$$

where N_c = number of inelastically scattered protons detected, N_n = number of nuclei/cm² in scatterer, F = number of protons incident upon scatterer, and $\Delta\Omega$ = solid angle accepted by counter telescope. From this we can compute expressions for $d\sigma/d\Omega$, using values for $\Delta\Omega$, N_n, and F given in the last section. The results are

$$(d\sigma/d\Omega)_{\mathrm{Pb}} = 6.53\times10^{-28} N_c/V,$$
$$(d\sigma/d\Omega)_{\mathrm{Au}} = 6.60\times10^{-28} N_c/V,$$
$$(d\sigma/d\Omega)_{\mathrm{Ta}} = 8.00\times10^{-28} N_c/V,$$
$$(d\sigma/d\Omega)_{\mathrm{Sn}} = 3.91\times10^{-28} N_c/V,$$

where V = voltage to which the Faraday cup electrometer circuit condenser is charged.

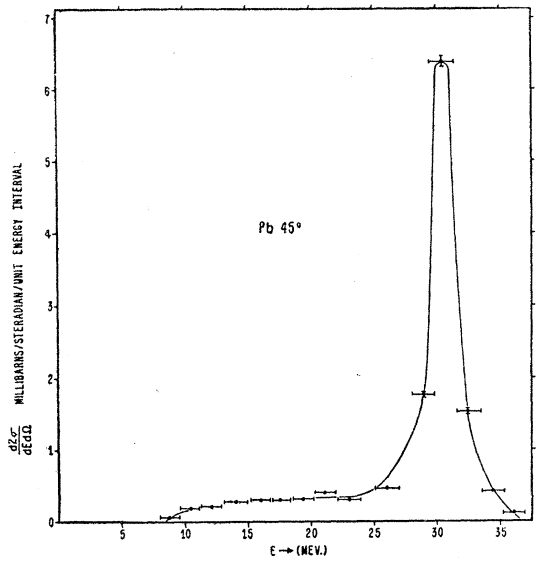

FIG. 9. Energy spectra of protons emitted by Pb at 45° when bombarded by 31-Mev protons.

The total cross section for a particular element may be calculated from the expression

$$\sigma = \int \frac{d\sigma}{d\Omega} d\Omega.$$

Since, in this experiment, information about the differential cross sections is obtained at only six angles, the integral must be approximated by a sum. To do this, the unit sphere is divided into six zones centered about the polar angles at which the differential cross sections were measured. The solid angle of each zone is computed and then the total cross section is calculated from the expression

$$\sigma = \sum_i \left(\frac{d\sigma}{d\Omega}\right)_i \Delta\Omega_i.$$

D. Discussion of Linearity, Errors, and Uncertainties

As a check on the ability of the equipment to provide a linear energy measurement, the energy spectrum of 31-Mev protons scattered from a C target was measured. The observed energy spectrum was in good agreement with the spectrum of Levinthal *et al.*,[5] which was obtained from range measurements. Since the peaks in each spectrum fell at the same energies, the apparatus must be linear.

To arrive at the total uncertainty in the measured cross sections due to the various sources of error, one first considers the formula for the differential cross section

$$\frac{d\sigma}{d\Omega} = \frac{N_c}{\Delta\Omega N_n F}.$$

The solid angle is calculated from the equation: $\Delta\Omega = \pi r^2/R^2$, where r is the radius of the collimator hole and R is the distance of the hole from the target. Both of these distances have a possible error of about 1 percent. Therefore $\Delta\Omega$ is uncertain to about 4 percent.

N_n, the number of target nuclei, is given by the expression: $N_n = (N_{\text{Avogadro}}/A)\sqrt{2}\rho$, where ρ is the areal density of the target. The mean density of the foil is known to about $\frac{1}{2}$ percent, but the density of the region of the foil bombarded by the beam is probably known to only about 2 percent.

F, the number of protons incident upon the scatterer, has uncertainty contributed from three sources: calibration and linearity of the integrating electrometer,

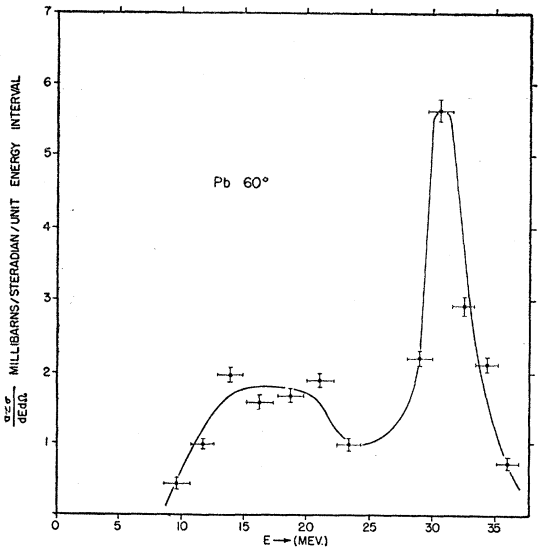

FIG. 10. Energy spectra of protons emitted by Pb at 60° when bombarded by 31-Mev protons.

calibration of the condenser in the circuit, and human error in throwing the "count-stop" switch at the proper time. The magnitude of these errors are estimated to be, respectively, $\frac{1}{2}$ percent, $\frac{1}{2}$ percent, and 1 percent.

N_c, the number of inelastically scattered protons, also has possible error contributed from three sources. First, there is the statistical fluctuation in the number of inelastically scattered protons counted. In all the spectra, the number of inelastically scattered protons is of the order of 1000, so the statistical errors are about 3 percent. Second, there is error involved in resolving the elastically and inelastically scattered protons. It is estimated that this error varies from about 3 percent for the 90° spectra to about 10 percent for the 30° spectra. Third, there is a source of error in the possible low-energy contamination of the beam and in possible slit scattering in the counter telescope. These effects constitute the largest source of uncertainty for the small angle differential cross sections and must be discussed in detail.

Collimator C_3, with all its baffles, was designed to minimize the possibility of slit-scattered protons of degraded energy from remaining in the beam and striking the scattering foil. However, the experiment is, by its very nature, extremely sensitive to beam contamination. This is because any low-energy component of the beam can Coulomb scatter from the target nuclei. At the small angles, the Coulomb scattering cross section becomes very large—and, at low energies, the $1/E^2$ dependence of the Coulomb cross section makes it even larger. Thus, at the forward angles, any low-energy beam contamination will have a high cross section for scattering into the counter telescope where it would be indistinguishable from inelastically scattered protons.

Similar spurious results would obtain if there were any appreciable amount of slit scattering in the collimator C_4 which defines the solid angle accepted by the counter telescope. This is because slit scattering of

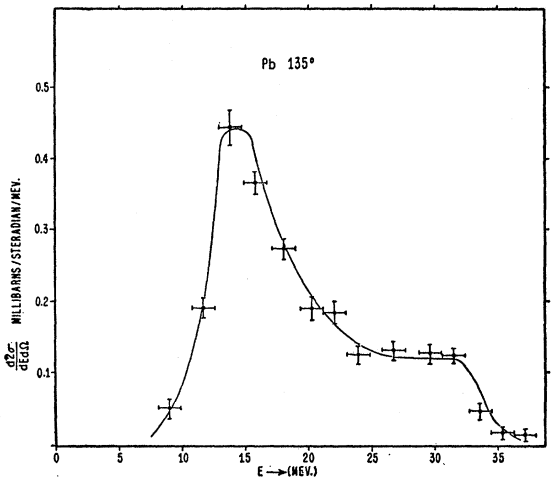

FIG. 11. Energy spectra of protons emitted by Pb at 135° when bombarded by 31-Mev protons.

elastically scattered protons would degrade their energy and cause them to be recorded by the scintillation counter as inelastically scattered protons.

To analyze the data, one must find some way to take these two effects into account. Fortunately this may be done unambiguously by using the 15° energy distributions as a background run. As an example, one would plot the 15° gold energy distribution on the same axes as the 30° gold energy distribution but with the ordinates contracted so that the area under the elastic peak of the 15° spectrum equals the area under the elastic peak of the 30° spectrum. Then the two curves would be very similar except that the low-energy part of the 15° spectrum contains approximately 50 percent of the area of the low-energy part of the 30° spectrum, i.e., the spectra have the appearance shown in Fig. 13.

Now, if one assumes that all of the low-energy part

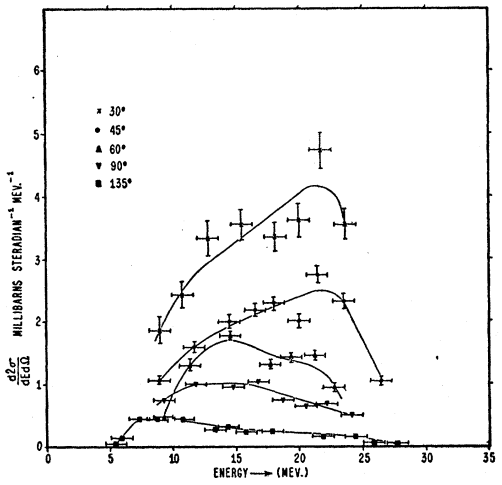

FIG. 12. Inelastically scattered protons emitted by Sn when bombarded by 31-Mev protons. The energy spectra at five scattering angles are shown.

of the 15° spectrum is due to slit scattering or beam contamination, then approximately 50 percent of the low-energy part of the 30° spectrum is due to real inelastically scattered protons, the rest being due to slit scattering or beam contamination. On the other hand, if one assumes that all of the low-energy part of the 15° spectrum is due to real inelastically scattered protons, then there can be no contribution from slit scattering or beam contamination to the 30° spectrum. Thus the true inelastic scattering cross section at 30° is bounded between 50 percent and 100 percent of the value indicated by the raw data.

Now the low-energy part of the 15° spectrum is certainly not all due to real inelastically scattered protons. Firstly, if it were, then the inelastic cross section would increase by about a factor of 20 in going from 30° to 15°. This does not correlate with the behavior of the differential cross section at other angles.

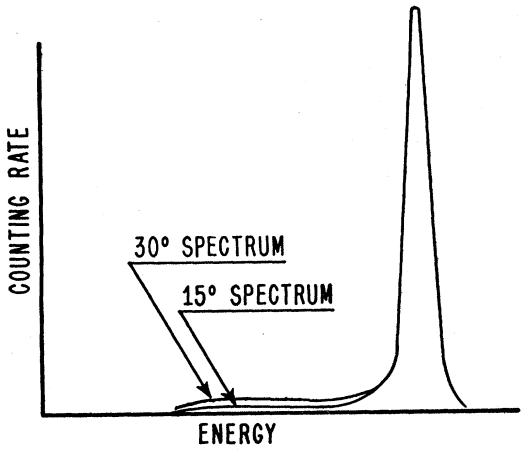

FIG. 13. Energy spectra of protons scattered at 15° and 30° from Au. The counting rates are normalized so that the elastic peaks contain an equal number of detected particles.

TABLE II. Estimated errors in the differential cross sections.

Angle	Errors which cancel in comparison of cross sections for various elements	Errors which will not cancel	Total error
30°	25%	11%	27%
45°	11%	8%	14%
60°	4%	6%	7%
90°	4%	5%	6%
135°	4%	5%	6%

Secondly, since, in the 15° spectrum, the counting rate per energy interval in the low-energy region is only about ½ percent of the counting rate per energy interval in the elastic peak, it is reasonable to expect that some of these low-energy protons are due to slit scattering or beam contamination. On the other hand, the low-energy part of the 15° spectrum is certainly not entirely due to slit scattering or beam contamination. This is true because at 30° these effects give roughly the same contribution to the spectrum as do real inelastically scattered protons and because the cross section for inelastic scattering of protons will be seen to be increasing fairly rapidly with decreasing angle at these angles.

Consequently, a reasonable estimate to make is that the correct value for the inelastic scattering cross section for gold at 30° lies somewhere near the center of the allowed range of 50 percent to 100 percent of the uncorrected value. Consideration of the other elements at 30° gives very similar results whereas at angles greater than 30° these effects are of rapidly decreasing importance.

At 30° the true value of the inelastic scattering cross section is taken to be 75 percent of the value given by the raw data. The limits of error are ±25 percent. At 45° the true value is taken to be 90 percent of the raw data value. The limits of error are ±10 percent. Beyond 45° these effects are negligible.

As is indicated above, the energy spectra taken at 15° are of little value in determining the true inelastic scattering cross sections. Consequently 15° cross sections will not be quoted in this paper. However, to determine the total cross section, an estimate of the 15° cross section must be obtained. This will be done by extrapolation from a smooth curve through the larger angle differential cross sections. This extrapolated value can be in error by as much as a factor of two.

To round up the discussion of uncertainties in the differential cross sections, it will be convenient to group the various sources of error into two types: (1) errors which would cancel out in a comparison of differential or total cross sections for the various elements, and (2) errors which would not cancel out in a comparison of the cross sections for the various elements. In the first group fall the sources of error due to $\Delta\Omega$, the electrometer, measurement of the condenser, and the error involved in the correction due to slit scattering and beam contamination. The second group consists of the errors due to measurement of the density of the scatterer, operation of "count-stop" switch, statistical fluctuations, and the resolving power of the scintillation. Table II gives the quadratic sums of the errors of each type and the quadratic sums of all errors.

The large values of the total probable error for the measurement of the differential cross sections at small angles reflects the fact that it is difficult to obtain information about a relatively small number of inelastic protons in the presence of an overwhelming number of elastic protons.

The error in the total cross section for inelastic scattering is calculated by taking a straight arithmetical average of the suitable weighted errors of the differential cross sections. The weighting factor, for a particular angle, is proportional to the product of the differential cross section and the solid angle for that angle. Since the actual values of the errors in the total cross sections depend on the shape of the differential cross section curve, these errors will not be quoted until the total cross sections are presented.

Since the total error involved in the measurement of a particular differential cross section is compounded from a number of sources of error which are independent, it is reasonable to compute the total error by taking a quadratic sum of the various contributing errors. However, it would not be correct to do the same in computing the error involved in the measurement of a total cross section since the total errors in the differential cross sections are not independent.

E. Differential Cross Sections

Table III lists the differential cross sections obtained in the experiment for the inelastic scattering of 31-Mev

TABLE III. Differential cross sections for the inelastic scattering of 31-Mev protons.

Element	Angle	N_c/V	$d\sigma/d\Omega$ mb/sterad	$d\sigma/d\Omega$ mb/sterad (corrected for slit scattering, etc.)
Pb	135°	644/100	4.2	4.2
	90°	919/40	15.0	15.0
	60°	1144/30	25	25
	45°	1496/20	49	44
	30°	1377/10	90	67
Au	135°	965/100	6.4	6.4
	90°	815/40	13.5	13.5
	60°	1076/30	24	24
	45°	...	...	...
	30°	1360/10	90	67
Ta	135°	698/100	5.6	5.6
	90°	647/40	13.0	13.0
	60°	750/30	20.0	20.0
	45°	1062/20	43	38
	30°	950/10	76	57
Sn	135°	2041/100	7.8	7.8
	90°	1427/40	14.0	14.0
	60°	1838/30	24	24
	45°	1965/20	38	35
	30°	1688/10	66	50

protons. The fourth column contains the data uncorrected for slit scattering and beam contamination. The fifth column is derived from the fourth column by applying the correction for slit scattering and beam contamination described in Sec. 4.

Figures 14 and 15 are plotted from the data contained in the fifth column of Table I. The errors indicated are of the type, described in the last section, which would not cancel out in a comparison of the differential or total cross sections of the various elements.

F. Total Cross Sections

Total cross sections are calculated according to the method described in Sec. 3. In order to do this, one must make estimates for the differential cross section for Au at 45° by interpolation and for the 15° cross sections for all the elements by extrapolation. The estimates are given in Table IV.

The results of the calculation of total cross section are given in Table V.

The probable error for the total cross sections, not including errors which would cancel out in taking the ratios of the total cross sections, is ±10 percent.

The probable error for any of the total cross sections, including all known sources of error, is (+25 percent, −20 percent). In this calculation, it was assumed that the actual value of the 15° cross section lies between twice and half the assumed value.

IV. CONCLUSIONS

This experiment provides three pieces of information: (1) the energy distribution of protons inelastically scattered from heavy elements, (2) the angular distribution for the inelastic scattering of protons from heavy elements, and (3) the total cross section for these

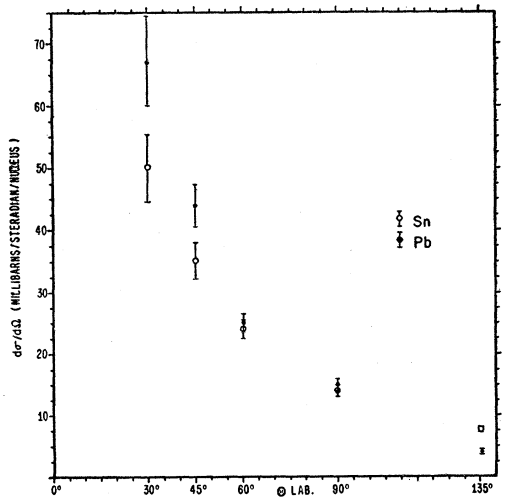

FIG. 14. Differential cross sections for the inelastic scattering of 31-Mev protons from Pb and Sn.

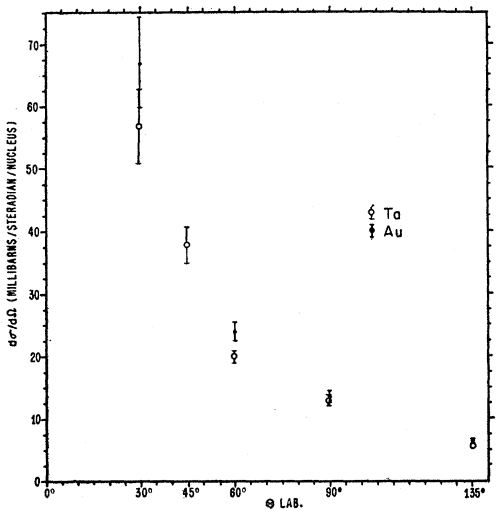

FIG. 15. Differential cross sections for the inelastic scattering of 31-Mev protons from Au and Ta.

inelastic scattering processes. All three point to one easily recognized conclusion—the inelastic scattering process which is taking place has nothing to do with the compound nucleus. The arguments involved in reaching this conclusion are:

(1) The relatively flat energy distributions are very different from the exponential distributions which would characterize the evaporation of nucleons from an excited compound nucleus.

(2) The angular distributions are strongly peaked forward (increasing by about a factor of ten in going from 135° to 30°). This is in contrast to the isotropic distribution one would expect from a compound nucleus process.

(3) The observed total cross sections, which are of the order of 15 percent of geometrical cross section, are at least an order of magnitude larger than the compound-nucleus cross section for boiling off protons through the Coulomb barrier of a heavy nucleus.

This conclusion does not imply that this is a case in which the compound-nucleus theory leads to incorrect results. Instead, what is apparently happening is that some additional process takes place which has a cross section so much larger than the compound nucleus cross section that the compound nucleus effects are completely hidden.

A model has been proposed which is capable of giving a qualitative explanation of the results of the experiment. According to the model, the inelastic scattering occurs when an incident proton collides with the rim of the nucleus.

Consider a 31-Mev proton incident upon a lead nucleus. The nucleus has a radius of $6r_0$, where $r_0=1.4\times10^{-13}$ cm. The incident proton has a de Broglie wavelength, λ, of $\frac{2}{3}r_0$. Consequently, it is legitimate to think of the proton as a small billard ball colliding with a larger billard ball, the nucleus. Now the mean free

path of a proton (or neutron) in nuclear matter has been calculated from the known nucleon-nucleon cross section by Serber.[14] At 30 Mev, his calculation indicates that the mean free path equals r_0. Thus, in any head-on collision with the nucleus, the incident proton will soon collide with the nucleons of the nucleus and rapidly share its kinetic energy with these nucleons. This event is just the one described by Bohr as being the first step in a compound nucleus process. However, in a collision in which the incident proton strikes the diffuse rim of the nucleus, it could collide with one or two nucleons in such a manner that either the incident proton or one of the struck nucleons would escape carrying away a relatively large fraction of the kinetic energy. The diffuse region at the rim of a nucleus, in which the nucleon density decreases from its value inside a nucleus to the external value of zero, is said[15] to have a thickness of the order of r_0. This fuzzy region should behave to some extent like a collection of free nucleons because of the reduced average nucleon density in the region. Consequently, the collision of the incident proton may be considered, approximately, as a collision between free nucleons.

TABLE IV. Extrapolated and interpolated cross sections used in calculating total cross sections.

Element	Angle	$d\sigma/d\Omega$ assumed mb/sterad
Au	45°	44
Pb	15°	110
Au	15°	110
Ta	15°	90
Sn	15°	70

The nucleon-nucleon collisions indicated by the model provide an explanation for the peaked forward character of the observed angular distributions. Consider a collision in which the incident proton strikes a nucleon at rest in the laboratory system. If the differential cross section for scattering is isotropic in the center-of-mass system of the two nucleons (a reasonable approximation for p-p or n-p scattering), then the differential cross section, in the laboratory system, will vanish in the backward hemisphere because of conservation of energy and momentum and will be proportional to the cosine of the scattering angle in the forward hemisphere. If, next, one allows the struck nucleon to have an initial momentum distribution provided by its proximity to the rest of the nucleons in the nucleus, the differential cross section indicated above may well smooth out into something similar to the experimental results shown in Figs. 14 and 15. For instance, the differential cross section would no longer vanish in the backward hemisphere since the incident proton may strike a nucleon with an initial backward component of momentum.

As a simple detailed-balancing argument would indicate, the exponential character of the energy distribution of nucleons emitted from a compound nucleus is essentially due to the exponential form of the energy dependence of the density of states of a nucleon bound to a nucleus. A calculation of the expected energy distribution for the nucleon-nucleon collision process indicated by the model would result in a similar theoretical description. However, in this case, the density of states to be used would probably be closely related to the density of states for a free particle. The density of states for a free particle (the familiar p^2dp factor) varies only slowly with energy. Consequently, the energy distribution would have only a relatively weak energy dependence (compared with an exponential dependence). This checks with the observed energy distribution.

By considering Figs. 7 through 11 one may see that the inelastic parts of the energy spectra are quite similar in shape. Furthermore, as Fig. 12 indicates, the maxima of the spectra shift toward higher energies at smaller scattering angles. These facts are in agreement with what one would expect from a nucleon-nucleon type process since the detailed shape of the energy spectra would not be sensitive to the atomic weight of the bombarded nucleus and since the more energetic particles would be prone to come off in the forward direction.

Finally, the model can be used to predict the magnitude of the total cross section and the dependence of the total cross section on the atomic weight of the nucleus.

The projected area of the diffuse rim is equal to the area of a ring of width r_0 and with a radius about equal to the radius R of the nucleus. The area of this ring is $r_0 \cdot 2\pi R$. The geometrical cross section of lead is equal to πR^2, where $R=6r_0$. The ratio of the area of the ring to the geometrical area of the Pb nucleus is thus one to three. The observed cross sections are approximately 15 percent of geometrical. Thus, the cross section for the process indicated by the model could well be large enough to account for the experimentally observed cross sections.

TABLE V. Total cross sections for the inelastic scattering of 31-Mev protons.

Element	σ_{total}, barns
Pb	0.29
Au	0.29
Ta	0.25
Sn	0.25

Since the projected area of the diffuse rim is proportional to the nuclear radius R and since nuclear radii are proportional to $A^{\frac{1}{3}}$, the total cross section for the

[14] R. Serber, Phys. Rev. 72, 1114 (1947).
[15] H. A. Bethe and R. F. Bacher, Revs. Modern Phys. 8, 164 (1936).

process predicted by the model might be expected to have an $A^{\frac{1}{3}}$ dependence. In going from Sn to Pb, $A^{\frac{1}{3}}$ increases by 20 percent. This agrees with the experimental evidence that the Pb total cross section is 15 percent greater than the Sn cross section.

The authors wish to express their appreciation to Professor Luis Alvarez for suggesting the problem and for stimulating guidance. In addition, we should like to thank the members of the crew of the Berkeley linear accelerator for their cooperation.

PHYSICAL REVIEW VOLUME 93, NUMBER 5 MARCH 1, 1954

The Half-Life of Lanthanum-140†

H. W. KIRBY AND MURRELL L. SALUTSKY
Mound Laboratory, Miamisburg, Ohio*

(Received September 17, 1953; revised manuscript received November 5, 1953)

Carrier-free lanthanum-140 was separated from barium-140 by a double barium nitrate precipitation from 80 percent nitric acid, using inert barium carrier. The half-life, determined by beta counting, was found to be 40.224±0.020 hours over a period of 574 hours.

IN a separate communication,[1] the authors describe a method for the separation of carrier-free lanthanum-140 from barium-140. A modification of this procedure was used to prepare a high-purity, high-specific activity product which would be suitable for use in a half-life determination.

As a preliminary purification, 0.5 gram of barium nitrate, spiked with approximately one millicurie of barium-140,[2] was precipitated from 80 percent nitric acid, and the filtrate was discarded. To remove possible strontium isotopes, the barium nitrate was redissolved, 10 milligrams of strontium carrier was added, and barium chromate was precipitated from homogeneous solution.[3] The filtrate, containing strontium chromate, was discarded. The barium chromate was redissolved, additional strontium was added, and barium chromate was again precipitated. The barium chromate was converted to barium nitrate (by precipitation from 70 percent nitric acid to remove chromate ion and residual strontium carrier).

The purified barium nitrate was set aside to allow time for the growth of lanthanum-140. After five days, the barium nitrate was precipitated from 80 percent nitric acid, and the filtrate, containing 85 percent of the lanthanum-140 and approximately 0.03 percent of the barium-140, was evaporated to dryness. The residue was redissolved in water, inert barium nitrate was added, and the precipitation was repeated. The filtrate was evaporated to dryness and redissolved in four milliliters of dilute nitric acid. The final solution contained approximately 0.7 millicurie of lanthanum-140, 10^{-7} millicurie of barium-140, and 50 micrograms of inert barium.

Since radium and lead isotopes, if present in the original barium-140, might have passed through the purification process, samples of the purified barium nitrate and the final lanthanum-140 solution were counted in an air-ionization parallel plate alpha counter having a background of less than one count per minute. No alpha counts were detected in either fraction or in any of the samples used for the half-life determination.

The instrument used for beta counting was a 2π proportional counter[4] having a resolution time of 0.1 microsecond. Samples were inserted in the windowless counting chamber, and the chamber was flushed thoroughly with a mixture of 90 percent methane and 10 percent argon. The gas flow was maintained throughout the counting period. The instrument was standardized daily with a plutonium standard sample, and the background, which varied between 50 and 75 counts per minute, was determined before and after each sample was counted. Background and coincidence corrections were made for all counting data. Each measurement was the average of two successive five-minute counts which agreed within one percent.

The upper limit of the instrument was approximately 350 000 counts per minute, and an arbitrary lower limit of approximately 1000 counts per minute was set to avoid loss of counting precision. With these restrictions, no single sample could be counted for more than eight half-lives. Accordingly, a special technique was used by which the lanthanum-140 decay could be followed for a much longer period.

Five samples of the lanthanum-140 solution were mounted on stainless steel disks and evaporated to dryness. The first sample contained approximately

† Abstracted from Mound Laboratory Report MLM-890, July 31, 1953. Available from Technical Information Service, Oak Ridge, Tennessee.

* Operated by Monsanto Chemical Company for the U. S. Atomic Energy Commission, Contract No. AT-33-1-GEN-53.

[1] M. L. Salutsky and H. W. Kirby, Anal. Chem. (to be published).

[2] Obtained from Isotopes Division, Oak Ridge National Laboratory, Oak Ridge, Tennessee.

[3] Salutsky, Stites, and Martin, Anal. Chem. 25, 1677 (1953).

[4] Nuclear Measurements Corporation Model PC-1 alpha-beta-gamma counter.

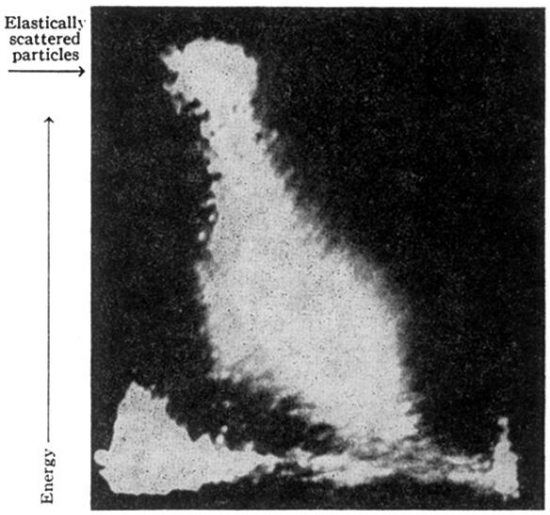

FIG. 6. Photograph of energy losses *vs* energies of particles emitted from a heavy element.